Assessment of FFD and CAD-based shape parametrization methods for adjoint-based turbomachinery shape optimization.

Conference Paper · May 2018

CITATIONS
8

READS
694

4 authors, including:

Nitish Anand
Delft University of Technology
12 PUBLICATIONS **46** CITATIONS
SEE PROFILE

Matteo Pini
Delft University of Technology
74 PUBLICATIONS **860** CITATIONS
SEE PROFILE

Piero Colonna
Delft University of Technology
155 PUBLICATIONS **3,336** CITATIONS
SEE PROFILE

Proceedings of Montreal 2018
Global Power and Propulsion Forum
7th - 9th May, 2018
www.gpps.global

GPPS-NA-2018-135

Assessment of FFD and CAD-based shape parametrization methods for adjoint-based turbomachinery shape optimization.

Nitish Anand
Propulsion and Power,
Delft University of Technology
N.Anand@tudelft.nl

Salvatore Vitale
Propulsion and Power,
Delft University of Technology
S.Vitale@tudelft.nl

Matteo Pini
Propulsion and Power,
Delft University of Technology
M.Pini@tudelft.nl

Piero Colonna
Propulsion and Power,
Delft University of Technology
P.Colonna@tudelft.nl

ABSTRACT

In automated design of turbomachinery, the method used to parametrize the blade shapes is key to ensure robustness and design flexibility of the entire optimization process. Typically, the two adopted methods are free-form deformation and computer-aided design based parametrization. The former allows for a large design flexibility, but it entails challenges to satisfy prescribed geometrical constraints. By contrast, the latter ensures a better control of the blade shape, but at the cost of narrowing down the design space. In this study, we aim at providing a unified methodology for a systematic assessment of the two methods by resorting to the adjoint method. A first comparison is conducted by carrying out shape optimization on a two-dimensional axial turbine cascade. The results indicate that, though the fluid-dynamic performance of the two optimal blade configurations are similar, the shapes are comparatively different, meaning that the optimization problem has multiple optima and that the type of parametrization is influencing the solution of the optimization problem.

INTRODUCTION

In recent time, the application of shape optimization methods to turbomachinery design has arguably peaked thanks to the unprecedented improvement of computer capabilities. Among the various optimization methods, the adjoint-based gradient method enables to handle design problems characterized by a large number of design variables in a very efficient manner (Pini et al., 2014) and to deal with multi-disciplinary and multi-physics design problems in turbomachinery (Martins et al., 2015).

One of the most critical, but often underestimated, aspects in automated design of turbomachinery is the choice of the blade shape parametrization method. Regardless the adopted optimization method, the parametric description of the baseline geometry is key to ensure robustness of the optimization process without hindering the capability of the design method to provide breakthroughs in shape configurations.

In the attempt to meet this objective, the Free Form Deformation (FFD) method has been recently applied to turbomachinery and gained increasing popularity over the well-established CAD-based method, especially for gradient-based optimization (Vitale et al., 2017; Verstraete et al., 2017). Although extremely flexible for exploring unconventional design solutions, the FFD method does not allow to directly control the blade geometrical characteristics (e.g., minimum thickness distribution, trailing-edge shape), leading often the optimizer to find blade shapes that cannot find real application. As consequence thereof, successful optimization with FFD is usually the result of trial and error endeavors aimed at adapting the FFD box to indirectly satisfy prescribed geometrical constraints.

By contrast, in CAD-based method, the blade geometry is parametrized with NURBS curves, whose control points position is derived by the geometrical characteristics of the blade, (e.g., the blade chord, the thickness distribution, the stagger angle). In this way, the attainment of feasible optimal shape is automatically ensured by bounding the design variables. This, however, comes at the cost of reducing the design space.

At present, both parametrization methods are indistinctly utilized in the context of adjoint methods, but no clear understanding of their strengths and weaknesses for turbomachinery

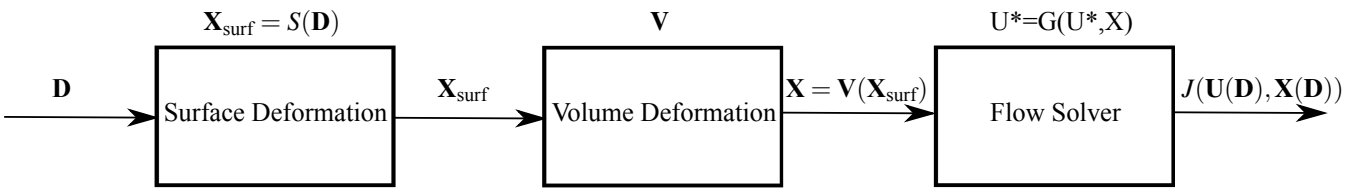

Figure 1 Schematic representation of fluid-dynamic design chain (Vitale et al., 2017).

applications has been gained yet. Stemming from this consideration, the objective of this work is to provide a unified methodology for a systematic assessment of i) the advantages and disadvantages of both methods and ii) their impact on the solution of the design problem, i.e. the final blade shape. A first comparison of the two parametrization methods is carried out by applying the proposed adjoint-based methodology to the design optimization of a two-dimensional axial turbine cascade.

The open-source CFD-suite SU2 (Economon et al., 2015) is used to carry out the comparison. The adjoint method available in the SU2 software, which was previously developed to solve turbomachinery shape-optimization problems with FFD (Vitale et al., 2017), is adapted to provide gradients information with respect to CAD-based design variables.

METHOD

The design chain of the shape optimization algorithm adopted in this work is summarized in Figure 1. A change in the design variables, $\mathbf{D}$, causes a variation of the blade shape, $\mathbf{X}_{\text{surf}}$, which in turn requires a continuous deformation of the volume mesh $\mathbf{X}$. The deformed mesh is then given as an input to the flow solver to compute the flow solution, $\mathbf{U}$, and to estimate the objective function $J(\mathbf{U}(\mathbf{D}), \mathbf{X}(\mathbf{D}))$.

Surface Deformation

Since the use of the surface nodes as design variables (i.e., $\mathbf{D} = \mathbf{X}_{surf}$) may lead to discontinuous solutions, a surface parametrization method, in which

$$\mathbf{X}_{surf} = \mathbf{S}(\mathbf{D}), \tag{1}$$

is adopted to guarantee that blade geometry is continuously deformed during the optimization process. Specifically in this work, two surface parametrization method are used. The first approach is based on the free-form deformation algorithms (Saderberg and Parry, 1986), while the other makes use of NURBS curves (Piegl and Tiller, 2012) typically used in CAD-based design methods.

Free-Form Deformation Parametrization

According to the FFD algorithm, the blade surface, included within the FFD box (see Figure 2), can be continuously deformed by displacing the FFD control points ($\mathbf{P}_{i,j}$). Consequently, $\mathbf{P}_{i,j}$ are chosen as the design variables, $\mathbf{D}$, of the optimization problem when the FFD algorithm is selected as parametrization method.

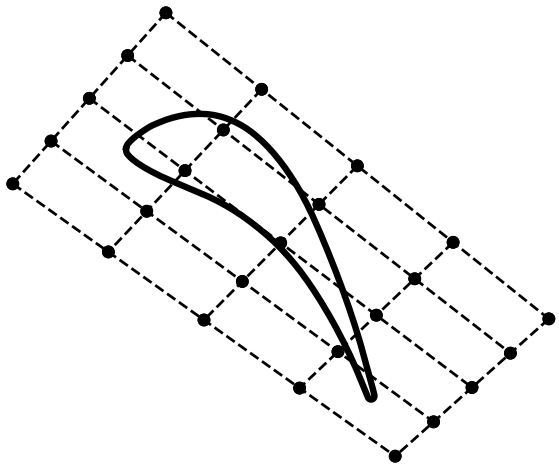

Figure 2 FFD-Type parametrization. Black dots depict the control points of the FFD Lattice.

The coordinate of the n-th point of the blade surface mesh at the k-th optimization step is given by

$$\mathbf{X}^k_{\text{surf},n} = \mathbf{X}^{k-1}_{\text{surf},n} + \Delta\mathbf{X}^k_{\text{surf},n}, \tag{2}$$

with

$$\Delta\mathbf{X}^k_{\text{surf},n} = \sum_{j=0}^{q}\sum_{i=0}^{o} B^o_i(d_n)B^q_j(g_n)(\mathbf{P}^k_{i,j} - \mathbf{P}^{k-1}_{i,j}), \tag{3}$$

where B^o_i and B^q_j are the i-th and j-th Bernstein polynomials, d_n and g_n are the values of the parametric coordinates in which the n-point of $\mathbf{X}_{\text{surf}}$ is mapped.

Computer Aided Design Parametrization

With the CAD-based approach a blade parametrization is obtained using typical turbomachinery design parameters (i.e., blade metal angles (β_{in},β_{out}), chord (c_{ax}), stagger angle (γ) and the pressure- and suction-side thickness distribution). These design variables are used to define a set of NURBS curves that will be used to construct the final blade shape. In this work, the construction and manipulation of the NURBS curves are performed using the openNURBS (Robert McNeel Associates, 1993) C++ library.

The procedure used to construct a generic 2D axial blade is shown in Figure 3. By fixing c_{ax} and γ, and selecting an arbitrary leading edge position (x_{LE}, y_{LE}), the trailing edge position

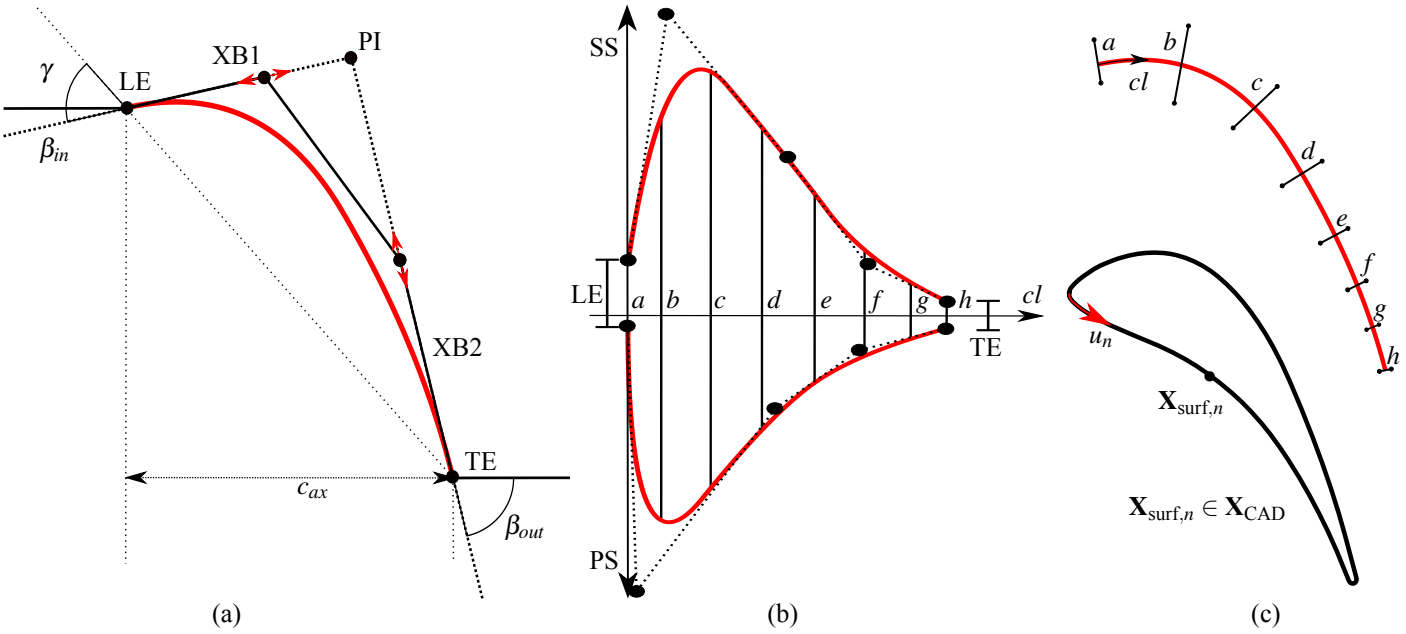

Figure 3 CAD-based parametrization. (a) Illustrates construction of camber-line using blade-characteristics, (b) Thickness distribution law for the pressure and the suction side (c) top - NURBS control-points for pressure and suction sides bottom - final blade geometry.

is univocally defined as

$$x_{\text{TE}} = x_{\text{LE}} + c_{\text{ax}}, \tag{4}$$

$$y_{\text{TE}} = y_{\text{LE}} + c_{\text{ax}} \tan(\gamma). \tag{5}$$

The intersection between the line departing from the LE with inclination β_{in} and the one departing from the TE in direction β_{out} defines the point PI. Once PI has been computed, the camberline can be defined using a NURBS curve composed of 4 control points LE, XB1, XB2, and TE, where the two internal points are customarily selected along the segments $\overline{\text{LEPI}}$ and $\overline{\text{PITE}}$. In this way, it is always guaranteed that the camberline curve exhibits a tangential value at the LE and TE in accordance with the corresponding metal blade angles (see Figure 3 (a)).

The thickness distribution laws for the suction- and pressure-side are defined with NURBS curves with an arbitrary number of control points (see Figure 3 (b)). These laws are, in turn, used to distribute in a equispaced manner another set of NURBS control points perpendicular to the camberline in order to define the blade suction- and pressere-side curves (see Figure 3 (c)). G^1 or G^2 continuity can be guaranteed at the intersection points of the suction- and pressure-side curves by appropriately distributing the suction and pressure-side control points around the LE and TE (Piegl and Tiller, 2012).

To summarize, the design variables, $\mathbf{D}$, used to univocally define the blade coordinates, $\mathbf{X}_{\text{CAD}}$, with the CAD-based approach are: β_{in}, β_{out}, c_{ax}, γ, the position of XB1 and XB2, and all the control points used to define the thickness distribution laws for the pressure- and suction-side. Thus, the relation between $\mathbf{X}_{\text{CAD}}$ and $\mathbf{D}$ can be mathematically expressed as,

$$\mathbf{X}_{\text{CAD}} = \mathbf{C}(\mathbf{D}, u), \tag{6}$$

where $\mathbf{C}$ represents all the algorithmic steps need to construct the blade, and u is the NURBS parametric coordinate.

In order to implement a procedure that is mesh-generation independent, it is generally assumed in this method that the blade representation within the mesh domain is mathematically different from the one constructed with the CAD-based model, i.e.

$$\mathbf{X}_{\text{surf}} \neq \mathbf{X}_{\text{CAD}}. \tag{7}$$

However, if $\mathbf{X}_{\text{CAD}}$ is constructed so that

$$\sqrt{\frac{\sum_{n=1}^{N} \left[\mathbf{X}_{\text{surf},n} - \mathbf{C}(\mathbf{D}, u_n)\right]^2}{N}} << 1, \tag{8}$$

it can be assumed that for each n-th point in the surface mesh

$$\Delta\mathbf{X}^k_{\text{surf},n} = \mathbf{X}^k_{\text{CAD},n} - \mathbf{X}^{k-1}_{\text{CAD},n} = \mathbf{C}(\mathbf{D}^k, u_n) - \mathbf{C}(\mathbf{D}^{k-1}, u_n) \tag{9}$$

where u_n represents the NURBS local parameter that maps the n-th point of $\mathbf{X}_{\text{surf}}$ into $\mathbf{X}_{\text{CAD}}$ using a minimum distance algorithm, and N is the total number of points in $\mathbf{X}_{\text{surf}}$.

Volume Deformation

Since re-meshing of the computational grid after each design step can be relatively CPU-expensive, the mesh deformation method presented in (Dwight, 2006) is applied. In this approach, the mesh is modeled as an elastic solid using the linear elasticity equations. Hence, if a surface deformation $\Delta\mathbf{X}_{surf}$ is imposed as Dirichlet condition, the mesh deformation $\Delta\mathbf{X}$ can be computed by solving the following linear systems:

$$\mathbf{K}\Delta\mathbf{X} = \mathbf{T}\Delta\mathbf{X}_{surf}, \tag{10}$$

where $\mathbf{K}$ is a constant stiffness matrix and $\mathbf{T}$ is projection matrix which re-orders $\Delta\mathbf{X}_{surf}$ in accordance with $\mathbf{X}$. The mesh corresponding to the next iterations k is then given by:

$$\mathbf{X}^k = \mathbf{X}^{k-1} + \Delta\mathbf{X}^k. \tag{11}$$

Flow Solver

As shown in (Vitale et al., 2017), $\mathbf{G}(\mathbf{U},\mathbf{X})$ is the *fixed point* operator that represents the time integration of the RANS equations according to an implicit Euler method, i.e.

$$\mathbf{U}^{n+1} = \mathbf{G}(\mathbf{U}^n, \mathbf{X}). \tag{12}$$

It is assumed that $\mathbf{G}$ is stationary only at feasible point $\mathbf{U}^*$ in which

$$\mathbf{R}(\mathbf{U}^*, \mathbf{X}) = 0 \Leftrightarrow \mathbf{U}^* = \mathbf{G}(\mathbf{U}^*, \mathbf{X}) \tag{13}$$

where $\mathbf{R}$ is the residual vector obtained from the spatial integration of the flow equations.

Sensitivities Computation

The optimization problem of the design chain describe above can be expressed as

$$\min_{D} \quad J(\mathbf{U}(\mathbf{D}), \mathbf{X}(\mathbf{D})), \tag{14}$$

$$\text{s.t.} \quad \mathbf{U} = \mathbf{G}(\mathbf{U}, \mathbf{X}), \tag{15}$$

$$\mathbf{X} = \mathbf{M}(\mathbf{D}) = \mathbf{V}(\mathbf{S}(\mathbf{D})). \tag{16}$$

Following the adjoint derivation approach with the Lagrangian multipliers, the adjoint equation and the mesh sensitivity equation can be written as

$$\bar{\mathbf{U}} = \frac{\partial}{\partial \mathbf{U}} J^T(\mathbf{U},\mathbf{X}) + \frac{\partial}{\partial \mathbf{U}} \mathbf{G}^T(\mathbf{U},\mathbf{X})\bar{\mathbf{U}}, \tag{17}$$

$$\bar{\mathbf{X}} = \frac{\partial}{\partial \mathbf{X}} J^T(\mathbf{U},\mathbf{X}) + \frac{\partial}{\partial \mathbf{X}} \mathbf{G}^T(\mathbf{U},\mathbf{X})\bar{\mathbf{U}}. \tag{18}$$

Once a numerical solution for the adjoint variables $\bar{\mathbf{U}}$ has been found, the mesh node sensitivity $\bar{\mathbf{X}}$ is computed from Eq. (18), and, the total derivative of J with respect to the design variables is given by

$$\frac{\mathrm{d}J}{\mathrm{d}\mathbf{D}}^T = \frac{\mathrm{d}}{\mathrm{d}\mathbf{D}} \mathbf{M}^T(\mathbf{D})\bar{\mathbf{X}}. \tag{19}$$

The volume deformation and the surface deformation routines must be differentiated in order to compute the final sensitivity $\frac{\mathrm{d}J}{\mathrm{d}\mathbf{D}}$, as

$$\frac{\mathrm{d}\mathbf{M}}{\mathrm{d}\mathbf{D}} = \frac{\mathrm{d}\mathbf{X}}{\mathrm{d}\mathbf{X}_{\text{surf}}} \cdot \frac{\mathrm{d}\mathbf{X}_{\text{surf}}}{\mathrm{d}\mathbf{D}}. \tag{20}$$

While $\frac{\mathrm{d}\mathbf{X}}{\mathrm{d}\mathbf{X}_{\text{surf}}}$ and $\frac{\mathrm{d}\mathbf{X}_{\text{surf}}}{\mathrm{d}\mathbf{D}}$ (only for the case of the FFD parametrization) are obtained using the algorithmic differentiation tool CodiPack , the surface sensitivity with respect to the design variables of the CAD-based method are computed using central finite difference scheme:

$$\frac{\mathrm{d}\mathbf{X}_{\text{surf}}}{\mathrm{d}\mathbf{D}} = \frac{\mathrm{d}\mathbf{X}_{\text{CAD}}}{\mathrm{d}\mathbf{D}} = \frac{\mathbf{C}(\mathbf{D}+\delta) - \mathbf{C}(\mathbf{D}-\delta)}{2\delta}. \tag{21}$$

The finite difference method is found to be accurate with a maximum variation of 0.001% with different values of δ. The gradient computation cost is negligible compared to the cost of one CFD run.

RESULTS AND DISCUSSION

The capabilities of the shape-optimization method described in the section above are demonstrated by redesigning a subsonic turbine stator. The selected stator geometry is the mid-span 2D section of the first stator from the 1 1/2 stage axial turbine, previously documented by Stephan et al. (2000). The flow-domain was discretized using an unstructured grid composed by 28000 grid elements, with hexahedral elements close to the wall and triangular in rest of the domain. The turbulent equations were closed with the k-ω SST turbulence model (Menter, 1993), ensuring wall $y+$ below unity along the blade surface. Lastly, the boundary conditions used for the the simulation are summarized in Table 1.

Table 1 Boundary conditions.

Fluid	Air	[-]
$T_{\text{tot,in}}$	305.7	[K]
$p_{\text{tot,in}}$	0.149	[MPa]
β_{in}	0.0	[°]
p_{out}	0.09	[MPa]
$I_{\text{tur,in}}$	0.03	[-]
$\left(\frac{\mu_{\text{tur}}}{\mu_{\text{lam}}}\right)_{\text{in}}$	100.0	[-]

A maximum number of 7000 iterations was set for both the flow and the adjoint solver in order to guarantee a reduction of 3 order of magnitude for the residuals of the adjoint equations (cf. Figure 4). For both solvers, the solutions were obtained by using an Euler implicit time-marching scheme with a CFL of 10 without resorting to the multi-grid acceleration technique.

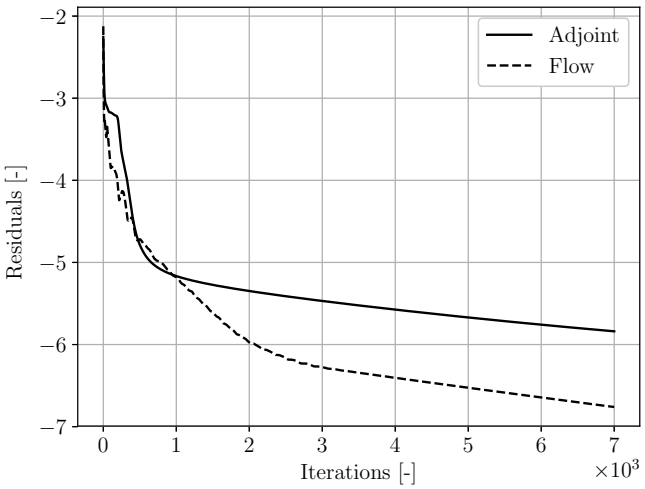

Figure 4 Convergence of the density conservative variable for the Flow and Adjoint solvers.

The stator was redesigned by solving the following optimization problem:

$$\min_{\mathbf{D}} \quad s_{\text{gen}}, \tag{22a}$$

$$s.t. \quad \beta_{\text{out}} > 70°. \tag{22b}$$

The entropy generation, s_{gen}, and the flow outlet angle, β_{out}, were computed using a mixedout average (Saxer, 1992) of the

flow quantities at the inlet and outlet boundaries. Specifically,

$$s_{\text{gen}} = \frac{s_{\text{out}} - s_{\text{in}}}{\frac{v_{\text{spout}}^2}{T_{\text{tot,in}}}}, \tag{23a}$$

$$\beta_{\text{out}} = \arctan\left(\frac{v_{\text{tang}}}{v_{\text{ax}}}\right)_{\text{out}}. \tag{23b}$$

Both parametrization method, FFD and CAD, are defined by 25 design variables. For the FFD method a box with 25 control points is used (cf. Figure 2), whilst the design variables for the CAD-based model are: β_{in}, β_{out}, γ, c, XB1, XB2, 10 NURBS CPs for suction-side thickness distribution law, and 9 CPs for the pressure-side (cf. Figure 3). In the following, optimal solution obtained from FFD parametrization will be referred to as FFD-Optimal and the one computed with CAD-based model as CAD-Optimal.

In both cases, the selected optimization method is the SLSQP algorithm (Kraft, 1988), a gradient based optimizer available in the SciPy library (Jones et al., 2001) within python. To guarantee a smooth convergence, the step size of the SLSPQ optimizer was under-relaxed with a value equal to 5E-04 for both the objective function sensitivity and the constraint sensitivity.

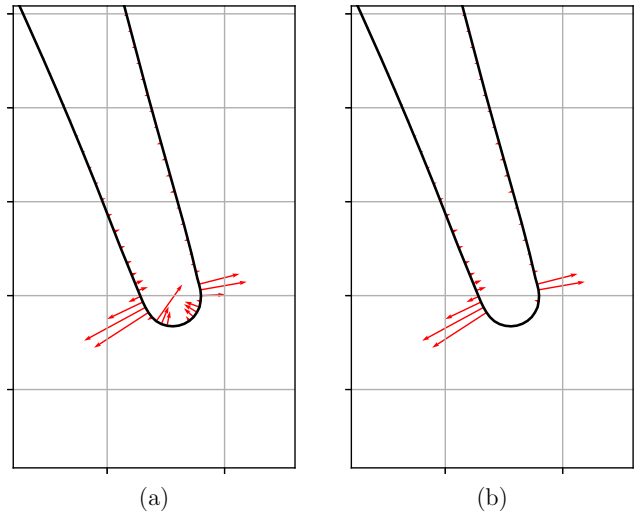

Figure 5 Sensitivities around the blade profile, (a) Actual TE Sensitivity (b) Nullified TE Sensitivity.

Finally, to prevent that the optimization converges to the trivial solution with a sharp trailing-edge, two different strategies were adopted. For the FFD case, the sensitivity around the trailing-edge was nullified at each optimization iteration (see Figure 5). For the CAD model, instead, the trailing-edge thickness was maintained by simply excluding the last NURBS control point of both the pressure- and suction-side thickness distributions from the optimization (cf. Figure 3 (b)).

Gradient Validation

The gradients of the objective functions with respect to the design variables of both parametrization methods were validated using the finite-difference scheme. For both FFD and CAD, a finite-difference step size of 1E-3 was selected. Figures 6 and 7 show that the gradient provided by the adjoint of design chain accurately correlate with sensitivities obtained with finite difference. This confirms that, although the adjoint equation are only resolved for three orders of magnitude, an accurate estimation of the gradient is obtained.

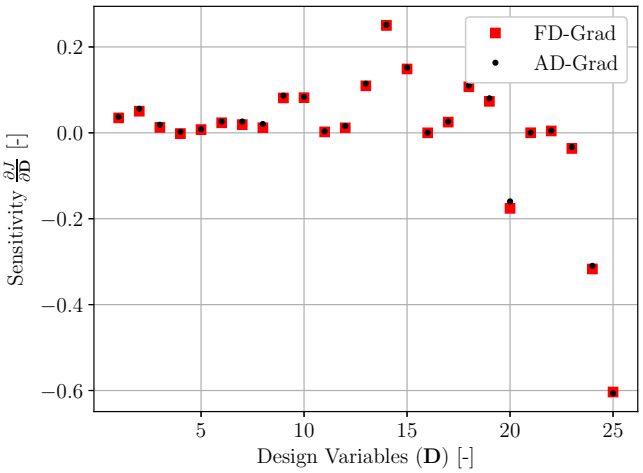

Figure 6 Gradient validation plot for FFD method, red represent finite-difference gradient solution and black represent Adjoint gradient.

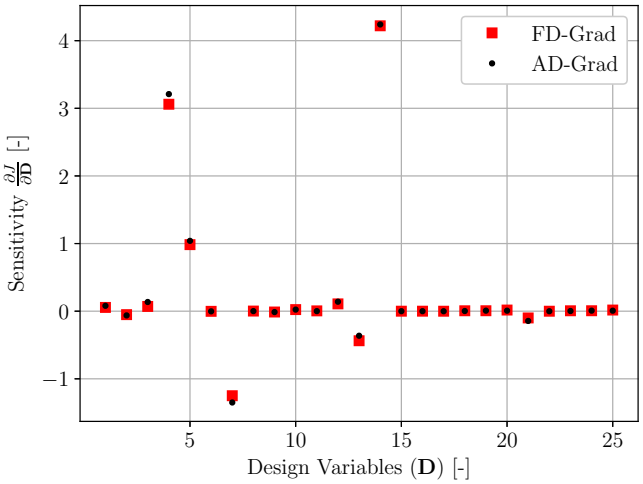

Figure 7 Gradient validation plot for CAD method, red represent finite-difference gradient solution and black represent Adjoint gradient.

Optimization

The normalized optimization history in Figure. 8 shows that both optimization processes converge within 15 iterations. In both cases, the entropy generation coefficient is reduced by approximately 10% and the inequality constraint on the outlet flow angle is satisfied. Figure 9 displays the baseline and the optimal blade profiles obtained with FFD and CAD. As can be observed, the optimization process leads to a more straight rear suction side and to a higher blade curvature in the front part

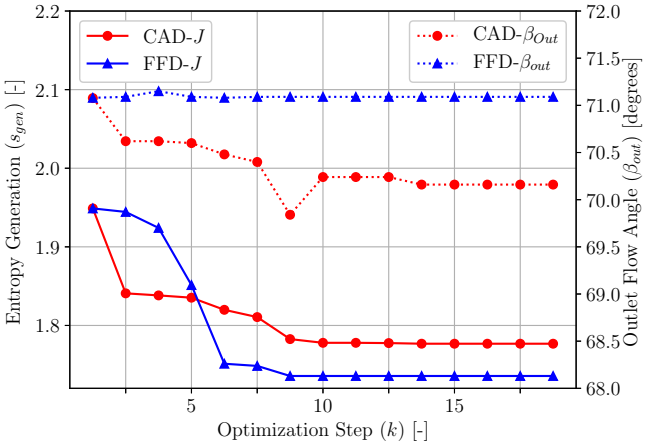

Figure 8 Convergence optimization history for both CAD and FFD methods.

of the suction side. The consequence thereof is a more pronounced flow acceleration in the vicinity of the cascade throat and a smoother deceleration towards the trailing-edge, which is highly beneficial to reduce boundary layer and trailing-edge losses. This is clearly visible in both the Mach contour and in the isentropic Mach number distribution along the blade surface, see Figure. 10 and 11. Furthermore, it is evident from Figure 10 the advantage offered by the CAD method in preserving the trailing-edge shape throughout the optimization process.

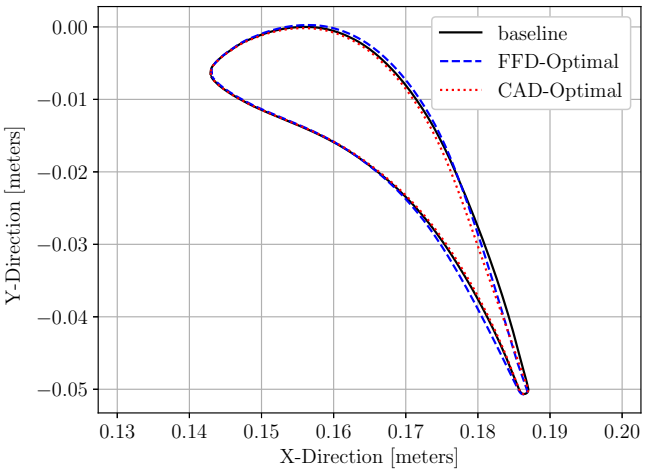

Figure 9 CAD vs FFD vs Baseline.

The advantage of adopting an optimization where the objective function is based on mixed-out averaging is apparent from Figure. 12, which shows the pitch-wise Mach number distribution downstream of the cascade. The optimal geometries ensure increased flow uniformity which allows to reduce the associated mixing-losses.

Although the fluid-dynamic performance of the optimal blade shapes are similar, the results provided by this design exercise point out two interesting considerations. i) Mathematically, the two parameterization methods lead the optimizer to converge to a different blade optimal shape, which indicates that the optimal solution depends on the parameterization method; ii) the optimization problem as described in Eq. (22) has multiple optima.

CONCLUSIONS

The present work documents an adjoint-based methodology to systematically assess the influence of the parametrization method on the optimal solution of turbomachinery design problems and their strengths and weaknesses for such applications. The study considered two types of parametrization methods, namely FFD boxes and CAD-based.

The methodology was applied by carrying out shape optimization on a two-dimensional turbine cascade. In light of the obtained results, the following final remarks can be drawn:

1. The use of FFD boxes ensure high degree of flexibility, but makes hard to respect prescribed geometrical constraints, for instance the trailing-edge thickness and shape.

2. For the same number of design variables, the FFD and CAD-based lead the optimizer to converge to optimal blades featuring similar fluid dynamic performance, but different shape. This is a clear indication that the optimal solution depends on the type of parameterization and, at the same time, that the constrained optimization problem as formulated in this paper presents multiple optima. In other words, the type of parametrization changes the mathematical relation underlying the specified optimization problem.

Further investigations are needed to gain insight of the dependence of the optimal configuration on the number of design variables and to draw best practices on the use of FFD and CAD-based parametrization methods for turbomachinery applications.

NOMENCLATURE

Symbols

B	Bernstein polynomial
$\mathbf{C}$	algorithmic step to construct blade
$\mathbf{D}$	design variables
$\mathbf{G}$	flow solver iterations
I	turbulence intensity
$\mathbf{J}$	objective function
$\mathbf{K}$	stiffness matrix
LE	leading edge
$\mathbf{M}$	mesh deformation matrix
N	number of surface points
$\mathbf{P}$	control points
PS	pressure side
PI	intersection point
$\mathbf{R}$	residual vector
$\mathbf{S}$	parametrization method
SS	suction side
$\mathbf{T}$	projection matrix
TE	trailing edge
T	temperature
$\mathbf{U}$	conservative variable vector

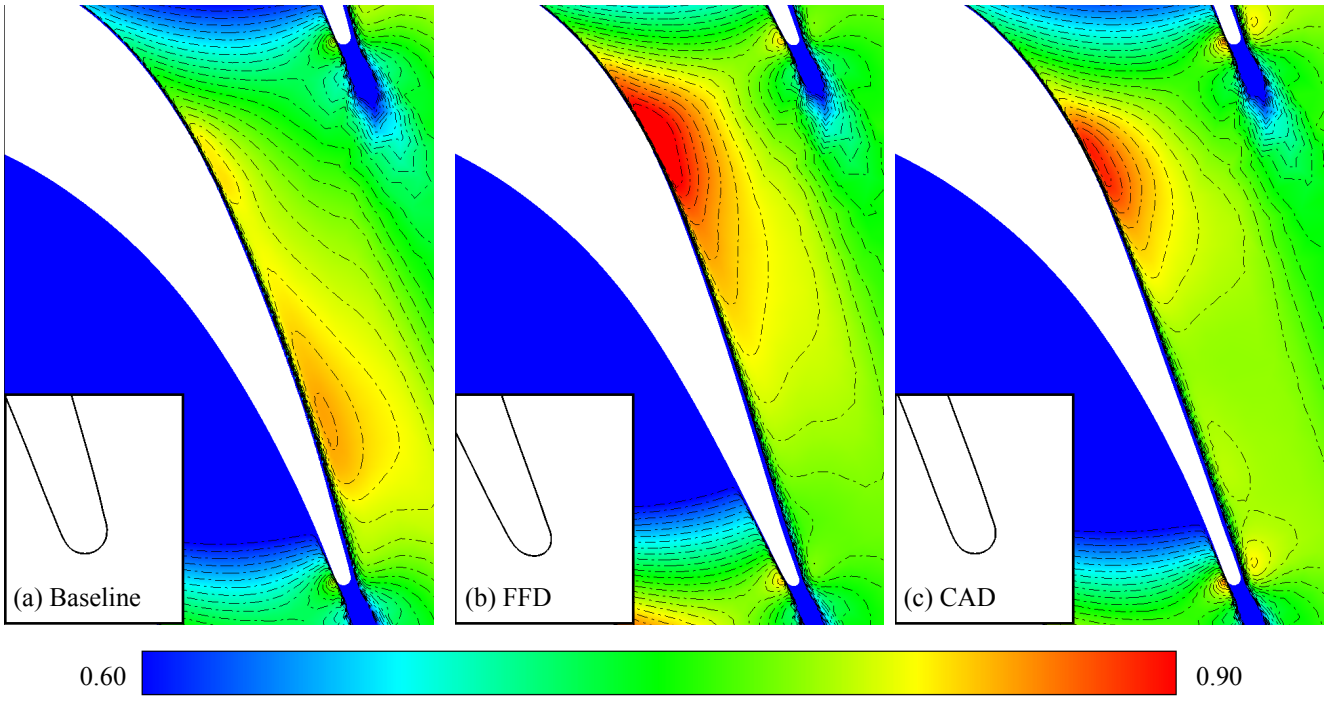

Figure 10 Mach contour.

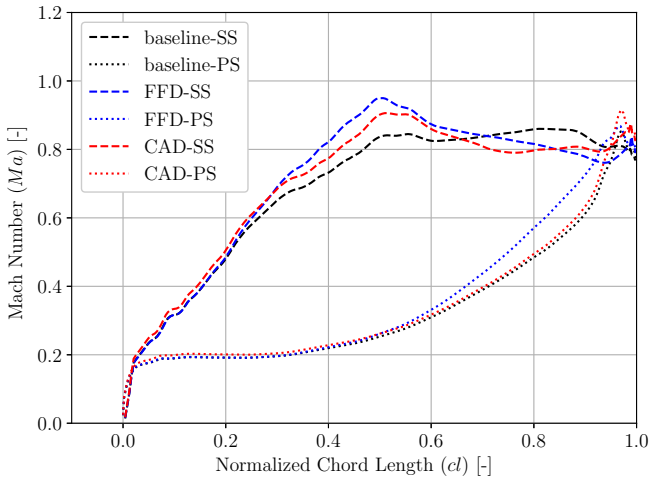

Figure 11 Isentropic Mach number distribution on the surface of baseline, CAD and FFD blade.

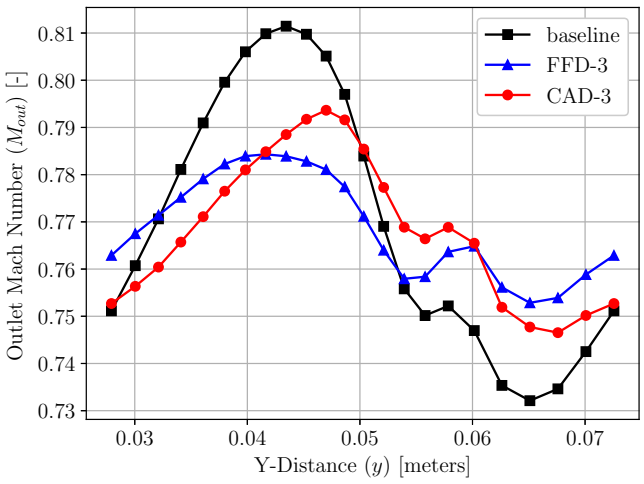

Figure 12 Pitch-wise Mach number distribution downstream of the cascade.

$\mathbf{V}$	volume
$\mathbf{X}$	vector of coordiantes
$a-h$	thickness distribution points
cl	camberline line distance
d, g	FFD co-ordinates
p	pressure
s	entropy
u	NURBS parametric coordinate
v	velocity magnitude
x, y	cartesian co-ordinates
z	loss coefficient

Greek letters

β	blade angle
δ	small difference
μ	viscosity
γ	stagger angle
Δ	difference

Superscripts

k	optimization step

Subscripts

CAD	Computer Aided Design
ax	axial
baseline	baseline

ext	extrapolated
gen	generation
i,j	numbers
in	inlet
is	isentropic
kin	kinetic
old	old
out	outlet
spout	spouting
surf	surface
tot	total conditions
tang	tangential
turb	turbulence
visc	viscous

REFERENCES

R. P. Dwight. Robust mesh deformation using the linear elasticity equations. *Computational Fluid Dynamics*, pages 401–406, 2006.

D. T. Economon, F. Palacios, S. R. Copeland, T. W. Lukaczyk, and J. J. Alonso. SU2: An open-source suite for multiphysics simulation and design. *AIAA Journal*, 54(3):828–846, 2015. doi: 10.2514/1.J053813.

E. Jones, T. Oliphant, P. Peterson, et al. SciPy: Open source scientific tools for Python, 2001. URL `http://www.scipy.org/`. [Online; accessed 5th January 2018].

D. Kraft. A software package for sequential quadratic programming. *Forschungsbericht - Deutsche Forschungs- and Versuchsanstaly fur Luft- and Raumfahrt*, 1988.

J. R. Martins, J. J. Alonso, and J. J. Reuther. A Coupled-Adjoint Sensitivity Analysis Method for High-Fidelity Aero-Structural Design. *Optimisation and Engineering*, 6: 33–62, 2015.

F. R. Menter. Zonal two equation k-ω turbulence models for aerodynamic flows. *24th AIAA Fluid Dynamics Conference*, 1993.

L. Piegl and W. Tiller. The NURBS book. *Springer Science & Business Media*, 2012.

M. Pini, G. Persico, D. Pasquale, and S. Rebay. Adjoint Method for Shape Optimization in Real-Gas Flow Applications. *Journal of engineering in Gas Turbine and Power*, 137(3), 2014. doi: 10.1115/1.4028495.

Robert McNeel Associates. OpenNURBs. *www.opennurbs.org*, 1993.

T. W. Saderberg and S. R. Parry. Free-form deformation of solid geometric models. *ACM SIGGRAPH computer graphics*, 20(4):151–160, 1986.

A. P. Saxer. A numerical analysis of 3-D inviscid stator/rotor interactions using non-reflecting boundary conditions. Technical report, Cambridge, Mass.: Gas Turbine Laboratory, Massachusetts Institute of Technology., 1992.

B. Stephan, H. E. Gallus, and R. Neihuis. Experimental Investigation of Tip Clearance flow and its influence on secondary flow in a 1-1/2 stage axial turbine. *Proceedings of ASME TurboExpo 2000, May 8-11, 2000, Munic Germany*, 2000.

T. Verstraete, L. Müller, and J.-D. Müller. CAD-Based adjoint optimization of the stresses in a radial turbine. *ASME Turbo Expo 2017: Turbomachinery Technical Conference and Exposition*, (GT2017-65005), 2017.

S. Vitale, T. A. Albring, M. Pini, N. R. Gauger, and P. Colonna. Fully turbulent discrete adjoint solver for non-ideal compressible flow applications. *Journal of the Global Power and Propulsion Society*, (Accepted), 2017.